Characterisation of mechanical insertion of commercial microneedles

Akmal H Sabri [a1], Zachary Cater [b1], Jane Ogilvie [c], David J Scurr [a], Maria Marlow [a] Joel Segal [d]*

[a.] Division of Advanced Materials and Healthcare Technologies, School of Pharmacy, The University of Nottingham, NG7 2RD, UK

[b.] Department of Mechanical, Materials and Manufacturing Engineering, Faculty of Engineering, University of Nottingham, Nottingham, NG8 1BB

[c.] Walgreens Boots Alliance, Thane Road, Nottingham, NG90 1BS

[d] Advanced Manufacturing Technology Research Group, Faculty of Engineering, University of Nottingham, Nottingham, NG8 1BB

Email address

[1]Joint First Authors: Akmal H Sabri and Zachary Cater

*Corresponding author: Dr Joel Segal: Joel.Segal@nottingham.ac.uk

Telephone: +44 0115 951 4012

Fax: 0115 951 3800

Keyword: Microneedle, skin strain, microchannels, biaxial stretch, skin insertion

Abstract

The protection provided by the human skin is mostly attributed to the *stratum corneum.* However, this barrier also limits the range of molecules that can be delivered into and across the skin. One of the methods to overcome this physiological barrier and improve the delivery of molecules into and across the skin is via the use of microneedles. This work evaluates the mechanical insertion of two different commercially available microneedle systems, Dermapen® and Dermastamp™. The influence of biaxial skin strain on the penetration of the two microneedle systems was evaluated *ex vivo* using a biaxial stretch rig. From the skin insertion study, it was apparent that for all levels of biaxial strain investigated, the Dermapen® required less force than the Dermastamp™ to puncture the skin. In addition, it was observed that the oscillating microneedle system, the Dermapen®, resulted in deeper skin insertion *ex vivo* in comparison to the Dermastamp™. The use of this new biaxial stretch rig and the *ex vivo* skin insertion depth study highlights that the oscillating Dermapen® required less force to perforate the skin at varying biaxial strain whilst resulting in deeper skin penetration *ex vivo* in comparison to the Dermastamp™. Although the Dermapen® punctured the skin deeper than the Dermastamp™, such difference in penetration did not influence the permeation profile of the model drug, imiquimod across the skin as evidenced from a 24-hour *ex vivo* permeation study.

38 # 1. Introduction

39 The human skin is the largest organ in the human body and is comprised of three layers; the epidermis,
40 dermis and hypodermis. The epidermis is a multilayer compartment of the skin that comprises of the
41 *stratum corneum* (SC)*, stratum granulosum, stratum spinosum* and *stratum basale* [1]. The outermost
42 layer of the epidermis, the *stratum corneum,* is avascular and has evolved to provide protection
43 against physical and chemical attack. The protection provided by the *stratum corneum* has also
44 resulted in a barrier to the delivery of compounds across the skin either for therapeutic or cosmetic
45 purposes [2].

46 Microneedles are one of the strategies explored to improve the delivery of compounds across the
47 skin. These are minimally-invasive needles with lengths that ranging between 250-1000 µm capable
48 of perforating the *stratum corneum* in order to promote the delivery of compound across the skin [3].
49 Due to their size, microneedles offer painless skin insertion as they are unlikely to stimulate the dermal
50 pain receptors upon application [4]. Some of the microneedle products available on the market,
51 licensed for cosmetic use, include the Dermastamp™ and Dermapen®.

52 The Dermastamp™ consists of a stamp with an array of microneedles arranged at the base of the
53 device. The microneedles are inserted into the skin in one vertical motion, creating micron sized
54 channels in the skin. The Dermapen® is a motor driven microneedling device that inserts its needles
55 into the skin in a continuous oscillating motion at one of five programmed frequency levels. The use
56 of a motor helps circumvent the issue of varying insertion force between users. It also features an
57 adjustable dial to control the needle's depth of penetration during use. However, little research exists
58 evaluating the effectiveness of such a motor driven device or the associated advantages or
59 disadvantages in its use in comparison to the Dermastamp™ and its single stamping motion.

In order to effectively generate microneedle channels, the skins topology must also be considered. The human skin features a roughened surface due to the variation in structure of the keratinocytes on the *stratum corneum* [5,6]. This surface is undulating in nature, being up to 150 microns from peak to trough for those aged over 60 [6], thus clearly demonstrating the need to smooth the skin as far as possible to maximise depth of penetration by the needles. To achieve smoothing, the skin must be stretched. It is understood that when skin is uniaxially stretched, the skin acts in a compressive fashion in the perpendicular direction to maintain the area of the surface, causing micro-furrows to develop [7].This highlights the need for biaxial stretching to mitigate against this and ensure microneedle insertion into the skin. Biaxial skin stretching has been performed in several studies [8–10] with a non-linear stiffening of skin being found as a function of strain. This relationship has been supported by a simulation study by Flynn and Rubin[11] however little other data appears to exist regarding how increase in strain affects the penetration of microneedle into the skin.

In this work, we compare the insertion force profiles of two commercially available microneedle systems; Dermastamp™ and Dermapen®. This study evaluates the influence of biaxial skin strain on the insertion force of two different microneedling systems into the skin. Besides that, the influence of microneedle oscillation during microneedle application was evaluated using an *in vitro* and an *ex vivo* set up.

2. Materials

Dermapen® (ZJChao, China) and Dermastamp™ (Teoxy Beauty, Wuhan, China). The Dermapen® is an oscillating microneedling pen featuring a 36-needle removable array, with tip radius of 44-68 µm and conical geometry. In order to mimic how the Dermapen® would be use by a patient in a real-world setting, the plastic ring around the microneedle cartridge was not removed for all skin insertion and permeation study. The Dermastamp™ is a non-oscillating microneedle stamp featuring a 42-needle

array of 1mm length, tip radius of 21-25 µm and curved conical geometry. The geometry of the microneedles from respective devices are visualised using Leica DM4000B (Leica Microsystem, Germany). The geometry of the microneedles is shown in Figure 1.

Porcine skin was used to study the insertion force profile of commercial microneedles instead of ex-vivo human skin due to its limited availability and the ethical difficulties associated with its use. Various studies have highlighted that porcine skin is a suitable alternative to human [12]. Porcine flank skin samples from six-month old animals were obtained from a local abattoir, reared specifically for food. Skin were collected prior to any steam cleaning, and then prepared. The skin was washed with distilled water and dried using tissue. Full thickness skin was used to avoid altering the skins biomechanical properties, which may lead to over-penetration of microneedles into the dermal tissue [13]. After that, the skin samples were stored at -20 °C and used within six months. Gentian violet solution 1% w/v (De La Cruz products, USA) was used as a dye to highlight the microneedle channels created in porcine skin. Parafilm M® (Brand Bermis, Wertheim, Germany) of 127 µm thickness was used as a skin simulant in the in-vitro insertion study. Imiquimod was purchased from Cayman Chemicals, USA. 5% w/w imiquimod cream (Aldara™), MEDA Company, Sweden was purchased from Manor pharmacy, UK. Sodium acetate was purchased from Sigma-Aldrich, UK. Acetonitrile (HPLC grade) and glacial acetic acid were obtained from Fisher Scientific, UK. Teepol solution (Multipurpose detergent) was ordered from Scientific Laboratory Supplies, UK. D-Squame standard sampling discs (adhesive discs) were purchased from Cuderm corporation, USA. Deionised water was obtained from an ELGA reservoir, PURELAB® Ultra, ELGA, UK. All reagents were of analytical grade, unless otherwise stated.

3. Methods

3.1. Biaxial Stretch Rig Development

Following two designs presented in literature [9,10], a low cost biaxial skin stretching rig was produced. The rig consists of four manual linear stages arranged as shown in Figure 2 on an 8 mm laser cut acrylic base. Further laser cut components permit clamping to be achieved using M4 Cap Head Bolts and 5mm acrylic plates. Friction between the clamping plates was improved using 40 grit emery cloth, double sided taped to the plates. The centre of the rig, over which the microneedle array is inserted, consists of an acrylic block topped with a 6mm layer of natural cork to simulate the stiffness of skeletal muscle [14] . Aluminium foil was overlaid on the cork with a thin covering of detergent. This was performed to reduce the friction experienced by the skin on the cork mat during stretching thus aiding the amount of strain that could be achieved within the skin. In addition, a laser cut jig for locating the biaxial stretch rig on the bed of a Texture Analyser (TA), (Stable Micro Systems, Surrey, UK) was also prepared to ensure consistency of the location of insertion of the microneedle array. Zero strain was assumed for each piece of skin when initially clamped.

3.2. Biaxial strain on microneedle skin insertion force

In order to investigate the effect of biaxial stretching on microneedle puncture performance of the Dermapen® and Dermastamp™, an insertion experiment was performed. The prepared porcine skin was inserted into the biaxial stretch rig and clamped, Figure 3 (a). The skin samples were then subjected to five levels of biaxial strain; 1.00, 1.0625, 1.125, 1.875 and 1.25 (i.e. a biaxial stretch of 0mm, 2.5mm, 5mm, 7.5mm and 10mm of a 40x40 mm grid). The level of biaxial strain was measured using a 40x40 mm grid of 5 mm squares ink-stamped onto the skin samples, Figure 3(a). The skin sample was biaxially stretched and a pair of Vernier callipers used to measure the level of stretch i.e. 0mm, 2.5mm, 5mm, 7.5mm and 10mm. Strain in each direction was calculated using Equation 1.

126 $$\varepsilon = \Delta l / l$$

127 Equation 1 - Equation for strain where ε is strain, l is length, and Δl is the change in length of skin. ε
128 strain, has no unit as the units from Δl and l cancel each other out.

129 The skin-loaded rig was then placed under the probe of the TA, using a laser cut jig to align a quadrant
130 with the probe's central position. A microneedle-loaded probe, see Figure 3(b), was then attached to
131 the TA. The following parameters were used for the TA program; 5kg Load Cell, Pre-Test Speed:
132 0.5mm/sec, Test Speed: 0.5mm/sec, Post-Test Speed: 10mm/Sec, Trigger Force: 0.01N. The
133 microneedles were inserted into the skin sample by the TA and the force-displacement profile
134 recorded. Following their removal, the Gentian Violet dye was applied to the skin, Figure 3(c) to
135 visualise the number of microneedle channels generated. The number of microchannels generated
136 were counted to measure the percentage of successful microneedle insertion. The Dermastamp™ was
137 housed in a custom mount that consist of a turned aluminium with a roll pin used to hold the
138 microneedle array in place. An M6 grub screw was used in the rear of the mount as an attachment to
139 the TA. For the Dermapen®, a 3D printed (Fused Deposition Modelling) jacket was designed to house
140 the device within an aluminium tube and stub assembly via a tapered interference fit. The assembly
141 was then attached to the TA again by an M6 grub screw. The Dermapen®'s adjustable needle length
142 was set to 1000 µm, the same length of the Dermastamp™ needles.

143 ### 3.3. *In vitro* skin simulant insertion study

144 As an alternative method to determine the microneedle penetration depth, a polymeric film (Parafilm
145 M®,) was used as a skin simulant. This insertion study was adopted from Larrañeta *et al.* 2014 [15]. In
146 brief, eight layers of Parafilm M® were stacked onto each other on a cork layer. Both microneedle
147 systems were applied onto the Parafilm M® stacks. Six replicates were performed, and the pores

148 generated were investigated under an optical microscope. The percentage of holes created per layer
149 for respective microneedle length was calculated using following Equation 2:

150 % hole generated: [(*N* microneedle channels observed)/ (*N* microneedles per array)] X 100

151 Equation 2 - Equation to establish the percentage of holes produced by the microneedle devices.
152 Where *N* represents 'number of'.

153 ### 3.4. *Ex vivo* skin insertion study

154 In order to evaluate the penetration depth of the Dermapen® and Dermastamp™ needles into the skin,
155 an *ex vivo* penetration study using porcine skin was conducted. The porcine flank skin was defrosted
156 at room temperature for an hour prior to the experiment. Using scissors, excess hair was carefully
157 trimmed from the skin. A 36-microneedle array tip was used, and the vibration speed was set to level
158 1 (412 cycles/min) [16]. The microneedle skin pre-treatment was applied by gently stretching the skin
159 and placing the Dermapen® vertically upon the skin for 10 seconds. A microneedle length of 1000 µm
160 was used in this study. After treating the skin with the microneedle pen, 10 µl of 1 % Gentian Violet
161 Dye was applied to the surface of the skin and left at room temperature for 60 minutes. Excess dye
162 was removed and the skin was then visually inspected to identify microneedle pores. The skin samples
163 were then cryo-sectioned (Leica CM3050 S Research Cryostat, UK) and the depth of microneedle
164 penetration was measured under an optical microscope (Zeta Profilometer, KLA-Tencor, US). The
165 same procedure was repeated to evaluate the depth of Dermastamp™ penetration into the skin.

166 ### *3.5. Skin permeation study*

167 In order to investigate the influence of the different microneedle system on skin permeation, an *ex*
168 *vivo* skin permeation study using a Franz-type diffusion cell was conducted using a model compound,
169 imiquimod. Imiquimod was selected as a model compound as the molecule displayed poor

170 permeation across the skin [2]. The application of microneedle system to skin is hypothesised to
171 improve the permeation of imiquimod into the skin. Prior to the permeation study, skin samples were
172 defrosted for at least an hour at room temperature. The skin was trimmed into small pieces according
173 to the surface area of the donor chamber of the Franz diffusion cell (Soham Scientific, Cambridgeshire,
174 UK). The trimmed skin samples were equilibrated by placing them above the receptor compartment
175 for 15 minutes prior to skin treatment. The porcine skins were subjected to the following treatment
176 modalities: i) application of 5% w/w of imiquimod cream alone as a control ii) application of 1000 µm
177 microneedles to the skin as a pre-treatment using Dermapen® followed by 5% w/w of imiquimod
178 cream iii) application of 1000 µm microneedles to the skin as a pre-treatment using Dermastamp™
179 followed by 5% w/w of imiquimod cream. Next, the porcine skins were placed on top of the receptor
180 compartment filled with 3 ml of degassed 100 mM acetate buffer pH 3.7. This buffer was selected as
181 the receptor phase in order to maintain a sink condition throughout the permeation study. This is due
182 to the insolubility of imiquimod at neutral or basic pH values. Various groups have reported the use of
183 acetate buffer pH 3.7 as the receptor phase in imiquimod permeation studies [17–19]. The skin was
184 then secured between the donor and receptor compartment of the diffusion cell using a metal clamp,
185 with the stratum corneum side facing the donor compartment. Upon assembling the Franz diffusion
186 cell, the permeation experiment was conducted over a period of 24 hours in a thermostatically
187 controlled water bath set at 36.5 ^{o}C.

188 After a 24-hour permeation experiment, the excess cream was removed and collected from the skin
189 surface by careful application of sponges soaked with 3% v/v Teepol® solution. The sponges were
190 pooled for imiquimod HPLC analysis as a total skin wash. Any formulation which might have spread to
191 the donor chamber was collected by the sponges and stored for imiquimod analysis by HPLC as a
192 donor chamber wash. Upon removing excess formulation from the skin surface, 15 sequential tape
193 strips were collected from the skin. The amount of imiquimod from the different Franz cell elements
194 (skin wash, donor chamber wash, pooled tape strips and remaining skin after tape stripping) were

195 extracted by the addition of 5, 5, 10 and 5 mL of methanol extraction mixture (Methanol 70%: Acetate
196 Buffer pH 3.7 100 mM 30%) respectively using a previously reported method [20]. Samples were then
197 vortexed for 1 minute and sonicated for 30 minutes before being left overnight. Subsequently,
198 samples were vortexed again and sonicated for a further 30 minutes. 1 ml of the extracts were
199 collected and spiked with 100 µl of 100 µg/ml propranolol as an internal standard. The samples were
200 then filtered through 0.22 µm membrane. For the receptor fluid, 1 ml of the solution from each Franz
201 cells were collected and spiked with 100 µl of 100 µg/ml propranolol as an internal standard before
202 being filtered through 0.22 µm membrane. HPLC analysis was carried out using an Agilent 1100 series
203 instrument (Agilent Technologies, Germany) equipped with degasser, quaternary pump, column
204 thermostat, autosampler and UV detector. System control and data acquisition were performed using
205 Chemostation software. The details of the HPLC chromatographic conditions are as follow: column
206 C18 (150 × 4.6 mm) ACE3/ACE-HPLC Hichrom Limited, UK. The mobile phase composition for analysis
207 of extracts from skin wash, donor chamber wash, pooled tape strips and remaining skin consists of 10
208 mM acetate buffer: acetonitrile (79:21). Whilst, the mobile phase composition for analysis of receptor
209 fluid consists of 10 mM acetate buffer: acetonitrile (70:30). The system operated at a flow rate of 1.0
210 mL/minute, UV detection at λ max=226 nm, injection volume of 40 µL and column temperature of
211 25 °C.

212

213 ### 3.6. *Statistical analysis*

214 All results were reported as the mean with standard error of mean (SEM) (n≥5). Statistical calculations
215 were performed in Prism (IBM, USA), a software package. The Student's t-test and One-Way ANOVA
216 followed by a Tukey HSD post-hoc test was applied to compare the results of different groups.
217 Statistically, a significant difference was denoted by p value < 0.05.

218 # 4. Results and Discussion

219 ## 4.1. Influence of biaxial strain on commercial microneedle perforation.

220 A biaxial skin stretching experiment was conducted in order to investigate the effect of skin strain on
221 the insertion of two commercial microneedle systems. From Figure 4 it can be seen that the force
222 needed by the Dermapen® to perforate the skin was significantly lower than the Dermastamp™ for
223 the range of strain rates investigated. It was also found that an increase in force was needed for the
224 Dermastamp™ to puncture the skin as the strain increased, however this force plateaued at a biaxial
225 strain of circa 1.1. In contrast, a linear relationship is presented for the Dermapen® suggesting that
226 insertion force increases with a higher strain rate.

227 The relationships shown in Figure 4, an increase in force with increases in biaxial strain, align with
228 Lanir & Fung's work that showed skin as a non-linear material that exponentially stiffens when biaxially
229 stretched [10]. As stiffness is defined as the resistance to bending or deformation, it is proposed that
230 as skin exponentially stiffens with an increase in strain. This results in the force needed to deform the
231 skin and insert the needles will increase significantly with biaxial stretching.

232 Following microneedle insertion, the formed puncture sites were visualised by application of Gentian
233 Violet Dye. The percentage of successful microneedle insertions is shown in Figure 5 for the two
234 microneedle systems. It is evident that as the biaxial strain of the skin sample increases, an increase
235 in the number of successful microneedle insertions was observed for the Dermapen®, which then
236 plateaus as the skin was subjected to further biaxial strain. For the Dermastamp™, as the biaxial strain
237 of the skin increases, we observed a rise in the percentage of successful microneedle insertion.
238 However, as biaxial strain of the skin was increased further, the percentage of successful microneedle
239 insertion into the skin decreased.

240 Previous work by Maiti *et al* has shown that subjecting the skin to strain may help smooth its surface
241 [21]. Such topographical change in skin structure may help mitigate the presence of micro-furrows on
242 the skin which fold around the microneedles and can present resistance to microneedle insertion [22].
243 One of the ways to achieve skin smoothening is via subjecting the skin to strain or stretching [23].
244 However, the current work suggests that smoothening the skin by subjecting the skin to biaxial strain
245 may help improve microneedle insertion up to an optimum strain (1.0625 and 1.125) as shown with
246 the Dermastamp™ in Figure 5. Beyond this optimum strain, the percentage of successful microneedle
247 penetration decreases due to increased skin stiffness with increasing strain as shown by previous
248 investigators [10].

249 For the Dermapen®, the increase in the percentage of successful microneedle insertions with
250 increasing strain is attributed to the observation that the skin smooths upon stretching [23].
251 Subjecting the skin to biaxial strain results in flattening of the micro-furrows and permits an increased
252 probability of the needles puncturing through the *stratum corneum*. This is due to the linear motor,
253 that oscillates the microneedle array, providing a secondary force to assist with insertion into the skin,
254 irrespective of the rise in skin stiffness with the increasing strain. These results demonstrate that the
255 Dermapen® is more effective than the Dermastamp™ in generating microneedle channels across the
256 skin.

257 Unlike the Dermastamp™, the presence of plastic shoulders at the tip of microneedle cartridge of the
258 Dermapen® imposes an additional surface tension to the skin during microneedle application. This
259 helps to further mitigate the propensity of the skin to fold around the needles while mitigating the
260 variability in puncture force. This is evidenced by the smaller standard deviation error bar for
261 Dermapen® relative to Dermastamp™ for the level of skin strain investigated shown in Figure *4*. The
262 combination of these physical factors mimics the insertion mechanism of a mosquito's proboscis. The
263 shoulder of the cartridge of the Dermapen® plays a similar role to that of the mosquito labium which

264 applies lateral strain to the skin prior to puncture. This ultimately focusses the force at the tip of the
265 Dermapen® permitting a more effective insertion [24]. The microneedles in this case are equivalent
266 to the mosquito's labrum which insert itself at defined frequency in a stamping manner allowing
267 deeper insertion with repeated insertion.

268 ### 4.2. *In vitro* skin simulant insertion depth study of commercial microneedle

269 An in-vitro skin simulant study, using Parafilm M®, was performed to compare the percentage of
270 successful microneedle channels against depth for the two commercial microneedle systems being
271 considered; the Dermapen® and Dermastamp™.

272 The insertion profiles of the commercial microneedle systems were established using a methodology
273 developed and validated by Larraneta *et al.* [15]. It involves the insertion of the microneedle devices
274 into a stack of eight Parafilm M® layers, followed by the separation of the layers and their visualisation
275 under an optical microscope to evaluate the number of microneedle channels formed, leading to the
276 insertion profiles in Figure 6.

277 The two microneedle systems typically pierce the first five layers, with approximately 100% of the
278 needles piercing the first three layers before the percentage of microchannels generated begins to
279 decrease. The generated channels displayed uniform geometry as shown in Figure 6 (a) and (b).
280 However, less than 50% of the microneedles successfully pierced the fifth and sixth layer.

281 Hutton *et al* showed that microneedle patches fabricated from a copolymer of methyl vinyl ether and
282 maleic acid were capable of penetrating the Parafilm M® layers to a depth of approximately 60% of
283 the microneedle height [25]. Vora *et al* also showed that microneedles fabricated from poly(vinyl
284 pyrrolidone) (PVP) loaded with nano- and microparticles were capable of penetrating the Parafilm
285 layers up to 60% of the microneedle length [26]. This work aligns with our findings that the commercial

286 microneedle systems were capable of penetrating Parafilm M® layers up to circa 60% of the
287 microneedle length. Furthermore, the results in Figure *6* (c) suggest that for an *in vitro* skin simulant
288 model, the insertion profiles are similar for both microneedle systems. In a follow up study, Larraneta
289 *et al* discovered that the insertion profile of microneedle arrays was more dependent on needle
290 density and design rather than the material used [27]. Such observations may explain the similar
291 insertion profiles of the two commercial microneedles systems, as both microneedles are made from
292 the same material; stainless steel.

293 ### 4.3. *Ex vivo* skin insertion study

294 An *ex vivo* penetration study was conducted to ascertain the microneedle penetration depth of the
295 two different commercially available microneedle systems in actual skin tissue. Figure 7 shows that
296 successful penetration of microneedles into *ex vivo* porcine flank skin evidenced from the visualisation
297 of microneedle channels from cryo-sectioned skin samples. From Figure 7 it was apparent that the
298 region surrounding the microneedle pore retained a normal structure with intact stratum corneum.
299 However, the microneedle channels displayed a deep indentation with disrupted *stratum corneum*.

300 In the context of drug delivery, it has been shown by Andrews *et al* that drug entry into and across the
301 skin is not just limited by the outermost layer of the skin, the *stratum corneum,* but the penetration
302 of molecules is limited by the overall epidermis itself [28]. This would suggest that both microneedle
303 systems were capable of perforating the skin to generate microneedle channels which could be used
304 by drug molecules to enter deeper layers of the skin.

305 It was evident that the microneedle penetration depth by the Dermapen® was significantly deeper in
306 comparison to the Dermastamp™. Such observation may be attributed to the oscillating motion of the
307 device during skin application which has been suggested to improve skin penetration [29]. Previous
308 work by Izumi *et al* investigated the influence of vibration on the penetration of microneedles into an

309 *in vitro* silicone skin model. The group observed that the application of vibrating microneedles at 30
310 Hz during skin application resulted in a reduction in the force needed to penetrate the skin [30]. This
311 reduction in puncture force is attributed to the reduction in effective frictional forces experienced by
312 microneedles under vibration [31]. The rapid vibration of the microneedles also mitigates the
313 likelihood of viscoelastic materials such as skin from attaching to the microneedle during the insertion
314 step. This reduction of effective frictional forces experienced by oscillating microneedles may also
315 serve as an explanation as to why the Dermapen® displayed lower peak insertion force in comparison
316 to the Dermastamp™, shown in Figure 4.

317 Another factor that may influence microneedle insertion into the skin is the different organization of
318 the microneedles on the Dermastamp and Dermapen systems. From Figure 7 (a) and (b) along with
319 microscopy image from Figure 6 (a) and (b) it is evident that the 36 microneedles on the Dermapen®
320 are organised in rows whereas the 42 microneedles on the Dermastamp™ are organised in concentric
321 circles. The needles on Dermapen® are closely distributed to one another in comparison to the needles
322 on the Dermastamp™. Previous work by Olatunji *et al* highlighted that insertion force increases with
323 when microneedle interspacing decreases [32]. In contrast to the finding by Olatunji *et al,* we observed
324 that although the needle interspacing on the Dermapen® are closer than the Dermastamp™, the
325 Dermapen® still required less insertion than the Dermastamp™. By comparing our findings to that of
326 Olatunji *et al*, it can be postulated that the method (oscillating vs non-oscillating) in which the
327 microneedle is applied to the skin overrides the influence of microneedle interspacing on insertion
328 force and penetration depth.

329 By comparing the penetration data for both microneedle systems from Figure 6 and Figure 7, it is
330 evident that the insertion of microneedles into *in vitro* skin simulant, Parafilm M® stacks, were
331 significantly deeper than that of *ex vivo* skin tissue. Such disparity in results suggest that the *in vitro*
332 test developed by Larraneta *et al* may have some limitations when the insertion data is translated to

333 *ex vivo* tissues and potentially *in vivo.* Both Parafilm M® and skin are inherently viscoelastic materials
334 which display both elastic and viscous properties under deformation. Unlike skin, which is an elastic
335 biological tissue that returns to its normal state after mild stretching or compression [33], Parafilm
336 M® exhibits irreversible plastic deformation when stretched or compressed [34].

337 ### 4.4. *Skin permeation study*

338 A permeation study was conducted to investigate the effect of different commercial microneedle
339 systems on the permeation of a model drug, imiquimod that displayed poor cutaneous permeation
340 [2]. One of the strategies to overcome the limited permeation of imiquimod is to employ permeation
341 enhancing strategy such as microneedle. Upon microneedle application, transient microchannels are
342 generated within the skin that promote the delivery of the drug across the skin. The amount of
343 imiquimod (µg) recovered from the various Franz cell components following the 24-hour permeation
344 study is displayed in Figure 8.

345 For all treatment modalities, we observed no statistical difference in the amount of imiquimod
346 recovered from different Franz cell components (donor wash, skin wash, tape strips and remaining
347 skin) except for the receptor fluid. With regards to receptor fluid, it was seen that when the skin was
348 pre-treated with either microneedle systems, we observed enhanced delivery of imiquimod across
349 the skin relative to the cream only control. However, it was worth noting we observed no statistical
350 difference in the permeation of imiquimod into the receptor fluid between Dermapen® and
351 Dermastamp™.

352 One possibility for the similarity permeation profile for the two microneedle systems is attributed the
353 fact that both systems successfully breached the *stratum corneum*, epidermis and down to superficial
354 dermis as highlighted in Figure 7 (c) and (d). It has been reported that thickness porcine epidermal
355 layer varies between 30-140 µm [35] and it was shown that both microneedle system penetrated into

356 the porcine skin to a depth of at least 200 µm, reaching the dermal layer of the skin. This layer of the
357 skin is viscoelastic due to the presence of a dense network of collagen and elastin [36–38]. Although
358 the Dermapen® may puncture the skin deeper than the Dermastamp™, immediately upon
359 microneedle removal the channels generated in the dermal layer of the skin immediately recoils and
360 reseals conferring similar resistance in permeation for imiquimod across the dermis for both
361 microneedle systems. A limitation which is frequently highlighted when a patch-and-poke strategy is
362 adopted for solid microneedles systems [39].

363 ## 5.0 Conclusion

364 In conclusion, this work expands our knowledge on the mechanical insertion of microneedles into the
365 skin. Applying biaxial strain on the skin indeed influences the penetration of microneedles into the
366 skin. It was apparent that the two commercially available microneedle systems, Dermapen® and
367 Dermastamp™ have very different insertion force profiles with increasing strain. For all the skin strain
368 levels investigated, it was evident that the Dermapen® required less insertion force than the
369 Dermastamp™. Interestingly, the percentage of successful insertion continues to increase before
370 plateauing with increasing skin strain for the oscillating Dermapen®. In contrast for the Dermastamp™,
371 the percentage of successful microneedle insertions increases with strain before decreasing at higher
372 strain rate. In terms of insertion depth, it was apparent that the penetration of the Dermapen® was
373 much deeper than that of the Dermastamp™. Such a difference was not detected when the
374 microneedle systems were evaluated using the commonly used Parafilm M® stack insertion study but
375 only became apparent when the devices were evaluated *ex vivo*. The lower insertion force and deeper
376 penetration provided by the Dermapen® was attributed to the oscillating feature of the microneedle
377 system which mitigates the effective frictional force experienced by the needle during skin insertion.
378 Lastly, although the Dermapen® may puncture the skin deeper than the Dermastamp™, such
379 difference in penetration did not affect the permeation profile of the model drug, imiquimod across
380 the skin as shown in the *ex vivo* permeation study.

Acknowledgements

This work was supported by the Engineering and Physical Sciences Research Council (EPSRC) [grant number: EP/L01646X/1] via a PhD sponsorship for Akmal Sabri; at the Centre for Doctoral Training for Advanced Therapeutics and Nanomedicine at the University of Nottingham. We would also like to thank Mr Ian Ward with the assistance on obtaining microscopy images of the microneedles for Figure 1.

Declaration of Competing Interest:

All the authors have no conflict of interest

References

[1] E. Candi, R. Schmidt, G. Melino, The cornified envelope: A model of cell death in the skin, Nat. Rev. Mol. Cell Biol. 6 (2005) 328–340. doi:10.1038/nrm1619.

[2] M.H. Al-Mayahy, A.H. Sabri, C.S. Rutland, A. Holmes, J. McKenna, M. Marlow, D.J. Scurr, Insight into imiquimod skin permeation and increased delivery using microneedle pre-treatment, Eur. J. Pharm. Biopharm. 139 (2019) 33–43. doi:10.1016/j.ejpb.2019.02.006.

[3] A.H. Sabri, J. Ogilvie, K. Abdulhamid, V. Shpadaruk, J. McKenna, J. Segal, D.J. Scurr, M. Marlow, Expanding the applications of microneedles in dermatology, Eur. J. Pharm. Biopharm. 140 (2019) 121–140. doi:10.1016/j.ejpb.2019.05.001.

[4] S. Kaushik, A.H. Hord, D.D. Denson, D. V Mcallister, S. Smitra, M.G. Allen, M.R. Prausnitz, Lack of Pain Associated with Microfabricated Microneedles, (2001) 2000–2002.

[5] M.M. Hurtado, M. Peppelman, X. Zeng, P.E.J. van Erp, E. Van Der Heide, Tribological behaviour of skin equivalents and ex-vivo human skin against the material components of artificial turf in sliding contact, Tribol. Int. 102 (2016) 103–113. doi:10.1016/j.triboint.2016.05.018.

[6] C. Edwards, R. Heggie, R. Marks, A study of differences in surface roughness between sun-exposed and unexposed skin with age, Photodermatol. Photoimmunol. Photomed. 19 (2003) 169–174. doi:10.1034/j.1600-0781.2003.00042.x.

[7] K. Nagano, G. Fyffe, O. Alexander, J. Barbič, H. Li, A. Ghosh, P. Debevec, Skin microstructure deformation with displacement map convolution, ACM Trans. Graph. 34 (2015). doi:10.1145/2766894.

[8] W.A. WA, Biaxial tension test of human skin in vivo., Biomed Mater Eng. 4 (1994) 473–86.

[9] J. Keyes, S. Borowicz, J. Rader, U. Utzinger, M. Azhar, J. Geest, Design and Demonstration of a Microbiaxial Optomechanical Device for Multiscale Characterization of Soft Biological Tissues with Two-Photon Microscopy, Microsc Microanal. 17 (2011) 167–75. doi:10.1007/978-1-4020-6754-9_17653.

[10] Y. Lanir, Y. Fung, Two-dimentional Mechanical Properties of Rabbit Skin - II Experimental Results, J. Biomech. 7 (1973) 171–182. doi:10.1016/0021-9290(74)90058-X.

[11] C. Flynn, M.B. Rubin, An anisotropic discrete fibre model based on a generalised strain invariant with application to soft biological tissues, Int. J. Eng. Sci. 60 (2012) 66–76. doi:10.1016/j.ijengsci.2012.04.006.

[12] F. Benech-Kieffer, P. Wegrich, R. Schwarzenbach, G. Klecak, T. Weber, J. Leclaire, H. Schaefer,

421 Percutaneous Absorption of Sunscreens in vitro: Interspecies Comparison, Skin Models and
422 Reproducibility Aspects, Skin Pharmacol. Physiol. 13 (2000) 324–335. doi:10.1159/000029940.

423 [13] Y.W. Naguib, A. Kumar, Z. Cui, The effect of microneedles on the skin permeability and
424 antitumor activity of topical 5-fluorouracil., Acta Pharm. Sin. B. 4 (2014) 94–99.
425 doi:10.1016/j.apsb.2013.12.013.

426 [14] M.M. Badran, J. Kuntsche, A. Fahr, Skin penetration enhancement by a microneedle device
427 (Dermaroller) in vitro: Dependency on needle size and applied formulation, Eur. J. Pharm. Sci.
428 36 (2009) 511–523. doi:10.1016/j.ejps.2008.12.008.

429 [15] E. Larrañeta, J. Moore, E.M. Vicente-Pérez, P. González-Vázquez, R. Lutton, A.D. Woolfson, R.F.
430 Donnelly, A proposed model membrane and test method for microneedle insertion studies,
431 Int. J. Pharm. 472 (2014) 65–73. doi:10.1016/j.ijpharm.2014.05.042.

432 [16] S. Bhatnagar, K. Dave, V.V.K. Venuganti, Microneedles in the clinic, J. Control. Release. 260
433 (2017) 164–182. doi:10.1016/j.jconrel.2017.05.029.

434 [17] R.F. Donnelly, P.A. McCarron, A.A. Zawislak, A. David Woolfson, Design and physicochemical
435 characterisation of a bioadhesive patch for dose-controlled topical delivery of imiquimod, Int.
436 J. Pharm. 307 (2006) 318–325. doi:10.1016/j.ijpharm.2005.10.023.

437 [18] C.G. Venturini, F.A. Bruinsmann, R. V. Contri, F.N. Fonseca, L.A. Frank, C.M. D'Amore, R.P.
438 Raffin, A. Buffon, A.R. Pohlmann, S.S. Guterres, Co-encapsulation of imiquimod and copaiba oil
439 in novel nanostructured systems: Promising formulations against skin carcinoma, Eur. J. Pharm.
440 Sci. 79 (2015) 36–43. doi:10.1016/j.ejps.2015.08.016.

441 [19] M. Sharma, G. Sharma, B. Singh, O.P. Katare, Systematically Optimized Imiquimod-Loaded
442 Novel Hybrid Vesicles by Employing Design of Experiment (DoE) Approach with Improved
443 Biocompatibility, Stability, and Dermatokinetic Profile, AAPS PharmSciTech. 20 (2019).
444 doi:10.1208/s12249-019-1331-1.

445 [20] D. De Paula, C.A. Martins, M.V.L.B. Bentley, Development and validation of HPLC method for
446 imiquimod determination in skin penetration studies, Biomed. Chromatogr. 22 (2008) 1416–
447 1423. doi:10.1002/bmc.1075.

448 [21] R. Maiti, L. Gerhardt, Z.S. Lee, R.A. Byers, A. Sanz-herrera, S.E. Franklin, R. Lewis, D. Woods, S.J.
449 Matcher, M.J. Carre, In vivo measurement of skin surface strain and sub-surface layer
450 deformation induced by natural tissue stretching, Journa l Mech. Behav. Biomed. Mater. 62
451 (2016) 556–569. doi:10.1016/j.jmbbm.2016.05.035.

452 [22] F.J. Verbaan, S.M. Bal, D.J. van den Berg, W.H.H. Groenink, H. Verpoorten, R. Lüttge, J.A.
453 Bouwstra, Assembled microneedle arrays enhance the transport of compounds varying over a
454 large range of molecular weight across human dermatomed skin, J. Control. Release. 117
455 (2007) 238–245. doi:10.1016/j.jconrel.2006.11.009.

456 [23] R. Maiti, L.C. Gerhardt, Z.S. Lee, R.A. Byers, D. Woods, J.A. Sanz-Herrera, S.E. Franklin, R. Lewis,
457 S.J. Matcher, M.J. Carré, In vivo measurement of skin surface strain and sub-surface layer
458 deformation induced by natural tissue stretching, J. Mech. Behav. Biomed. Mater. 62 (2016)
459 556–569. doi:10.1016/j.jmbbm.2016.05.035.

460 [24] S. Aoyagi, H. Izumi, M. Fukuda, Biodegradable polymer needle with various tip angles and
461 consideration on insertion mechanism of mosquito's proboscis, Sensors Actuators A Phys. 143
462 (2008) 20–28. doi:10.1016/j.sna.2007.06.007.

463 [25] A.R.J. Hutton, H.L. Quinn, P.J. Mccague, C. Jarrahian, A. Rein-weston, P.S. Co, E. Gerth-guyette,
464 D. Zehrung, E. Larrañeta, R.F. Donnelly, Transdermal delivery of vitamin K using dissolving
465 microneedles for the prevention of vitamin K de fi ciency bleeding, Int. J. Pharm. 541 (2018)
466 56–63. doi:10.1016/j.ijpharm.2018.02.031.

467 [26] L.K. Vora, R.F. Donnelly, E. Larrañeta, P. González-Vázquez, R.R.S. Thakur, P.R. Vavia, Novel
468 bilayer dissolving microneedle arrays with concentrated PLGA nano-microparticles for targeted
469 intradermal delivery: Proof of concept, J. Control. Release. 265 (2017) 93–101.
470 doi:10.1016/j.jconrel.2017.10.005.

471 [27] E. Larrañeta, R.E.M. Lutton, A.J. Brady, E.M. Vicente-Pérez, A.D. Woolfson, R.R.S. Thakur, R.F.
472 Donnelly, Microwave-assisted preparation of hydrogel-forming microneedle arrays for
473 transdermal drug delivery applications, Macromol. Mater. Eng. 300 (2015) 586–595.
474 doi:10.1002/mame.201500016.

475 [28] S.N. Andrews, E. Jeong, M.R. Prausnitz, Transdermal delivery of molecules is limited by full
476 epidermis, not just stratum corneum, Pharm. Res. 30 (2013) 1099–1109. doi:10.1007/s11095-
477 012-0946-7.

478 [29] M.T.C. Mccrudden, E. Mcalister, A.J. Courtenay, P. Gonz??lez-V??zquez, T.R. Raj Singh, R.F.
479 Donnelly, Microneedle applications in improving skin appearance, Exp. Dermatol. 24 (2015)
480 561–566. doi:10.1111/exd.12723.

481 [30] H. Izumi, T. Yajima, S. Aoyagi, N. Tagawa, Y. Arai, M. Hirata, S. Yorifuji, Combined harpoonlike
482 jagged microneedles imitating Mosquito's proboscis and its insertion experiment with
483 vibration, Electr. Eng. Japan. 3 (2008) 425–431. doi:10.1002/tee.20295.

[31] Y. Yokoyama, S. Okabe, Reduction of kinetic friction by harmonic vibration in an arbitrary direction, Bull. JSME-Japan Soc. Mech. Eng. 14 (1971) 139–146.

[32] O. Olatunji, D.B. Das, M.J. Garland, L. Belaid, R.F. Donnelly, Influence of Array Interspacing on the Force Required for Successful Microneedle Skin Penetration: Theoretical and Practical Approaches, J. Pharm. Sci. 102 (2013) 1209–1221. doi:10.1002/jps.23439.

[33] X. Xiang, F. Yan, Y. Yang, Y. Tang, L. Wang, J. Zeng, L. Qiu, Quantitative Assessment of Healthy Skin Elasticity: Reliability and Feasibility of Shear Wave Elastography, Ultrasound Med. Biol. 43 (2017) 445–452. doi:10.1016/j.ultrasmedbio.2016.10.002.

[34] L. Valentini, S. Bittolo Bon, M.A. Lopez-Manchado, L. Mussolin, N. Pugno, Development of conductive paraffin/graphene films laminated on fluoroelastomers with high strain recovery and anti-corrosive properties, Compos. Sci. Technol. 149 (2017) 254–261. doi:10.1016/j.compscitech.2017.06.023.

[35] L.K. Branski, R. Mittermayr, D.N. Herndon, W.B. Norbury, O.E. Masters, M. Hofmann, D.L. Traber, H. Redl, M.G. Jeschke, A porcine model of full-thickness burn, excision and skin autografting, Burns. 34 (2008) 1119–1127. doi:10.1016/j.burns.2008.03.013.

[36] J. Aziz, H. Shezali, Z. Radzi, N.A. Yahya, N. Hayaty, A. Kassim, J. Czernuszka, M.T. Rahman, Molecular Mechanisms of Stress-Responsive Changes in Collagen and Elastin Networks in Skin, Ski. Pharmacol Physiol. 629 (2016) 190–203. doi:10.1159/000447017.

[37] R. A.M., B. D.L., J.A. Bouwstra, B. F.P.T, O. C.W.J, Monitoring the penetration process of single microneedles with varying tip diameters, J. Mech. Behav. Biomed. Mater. 40 (2014) 397–405. doi:10.1016/j.jmbbm.2014.09.015.

[38] W. Martanto, J.S. Moore, T. Couse, M.R. Prausnitz, Mechanism of fluid infusion during microneedle insertion and retraction, J. Control. Release. 112 (2006) 357–361. doi:10.1016/j.jconrel.2006.02.017.

[39] Y.C. Kim, J.-H. Park, M.R. Prausnitz, Microneedles for drug and vaccine delivery, Adv. Drug Deliv. Rev. 64 (2012) 1547–1568. doi:10.1016/J.ADDR.2012.04.005.

Figures and legends

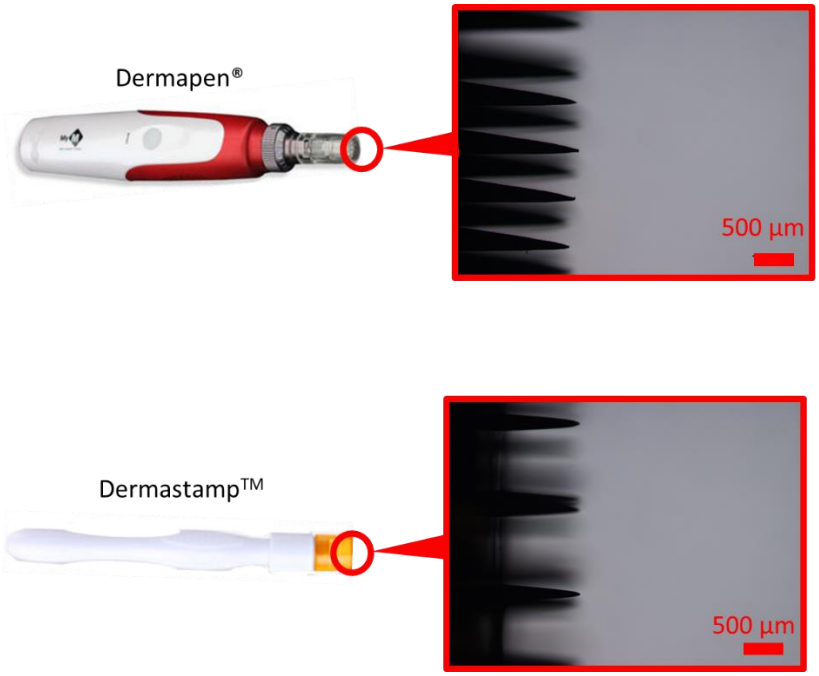

Figure 1 Close up microscopy image showing the geometry of microneedles from Dermapen® and Dermastamp™

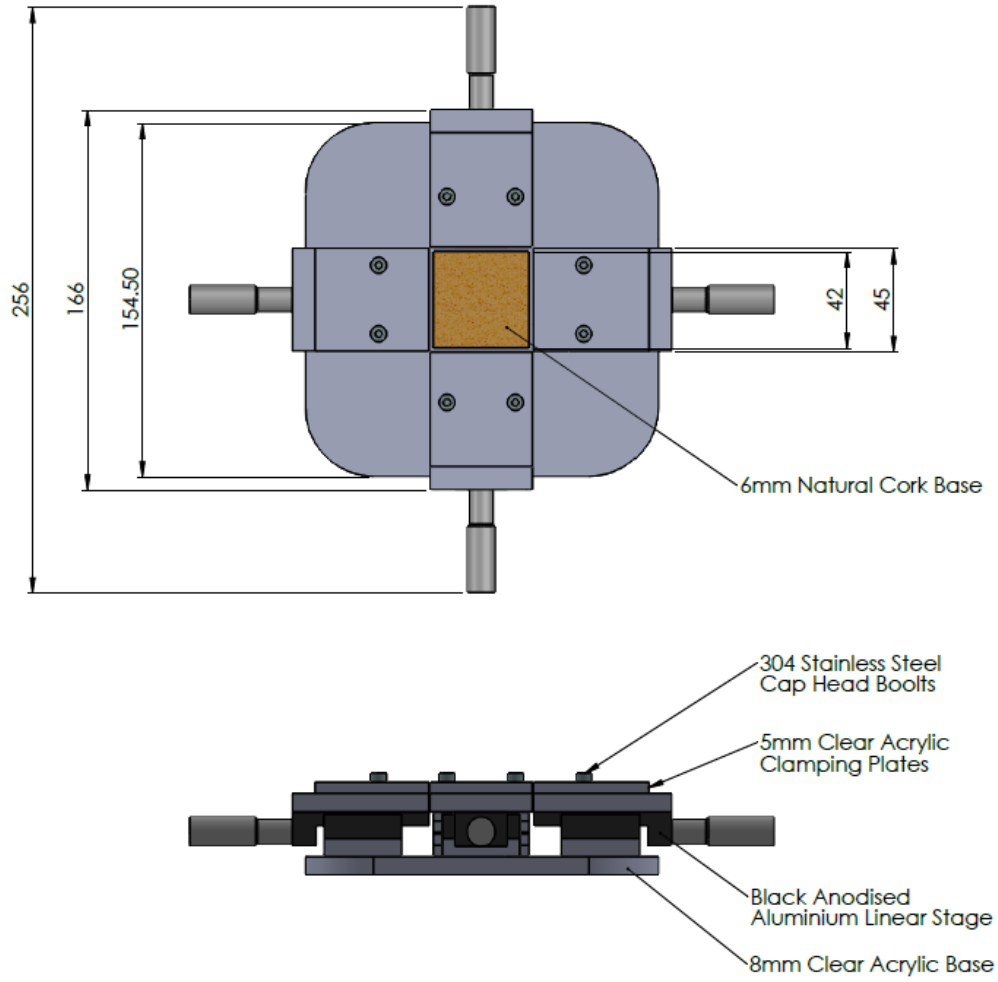

Figure 2 - A schematic of the conceived manual biaxial stretch rig

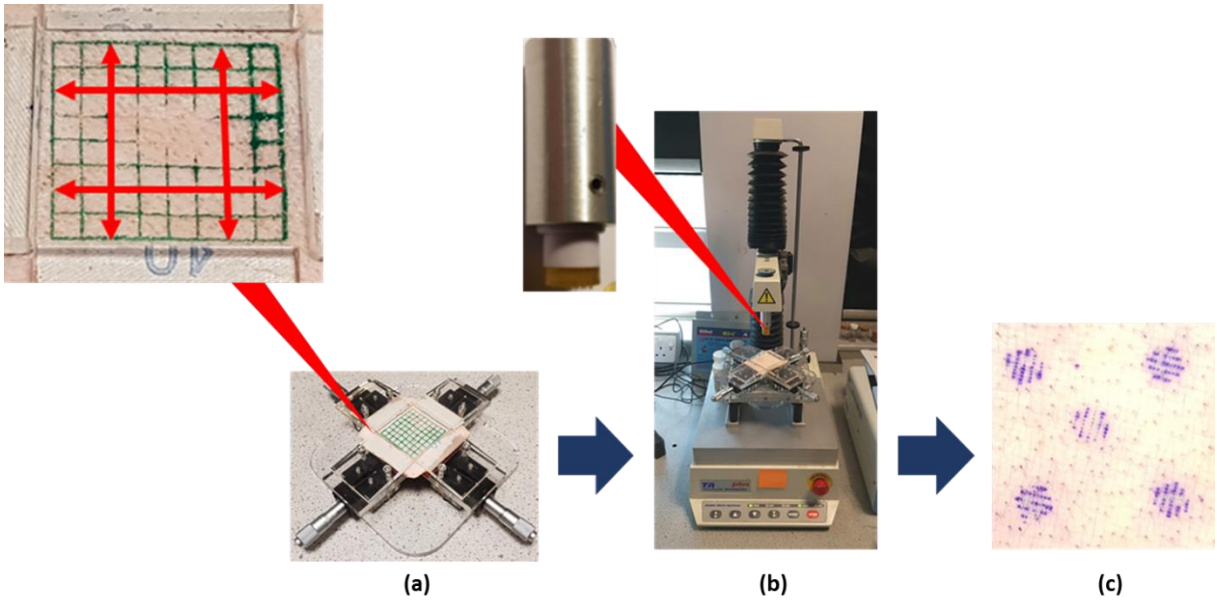

Figure 3 - Schematic detailing the setup to investigate effect of biaxial strain on microneedle skin insertion. A 40x40 mm grid of 5 mm squares ink was stamped onto the skin samples in **Step (a)** in order to measure the level of biaxial strain on the skin. Using a texture analyser (TA), respective microneedle systems were attached to the probe of the instrument to allow insertion into the skin as shown in **Step (b)**. Visualisation of microneedle channels using Gentian Violet dye as depicted in **Step (c)**

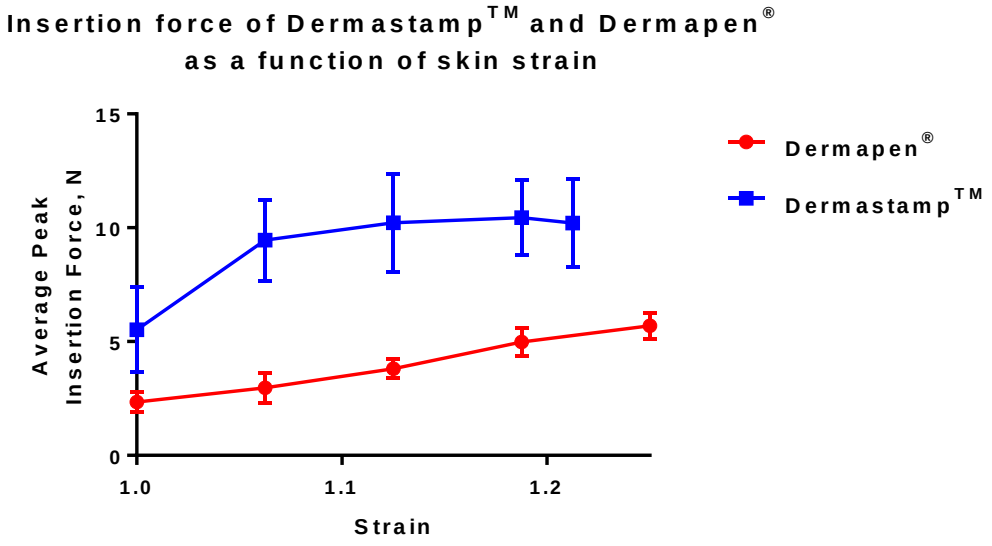

Figure 4 Biaxial skin strain and insertion force relationship for commercial microneedle systems Dermapen® and Dermastamp™. Data expressed as means ± SD, n=5.

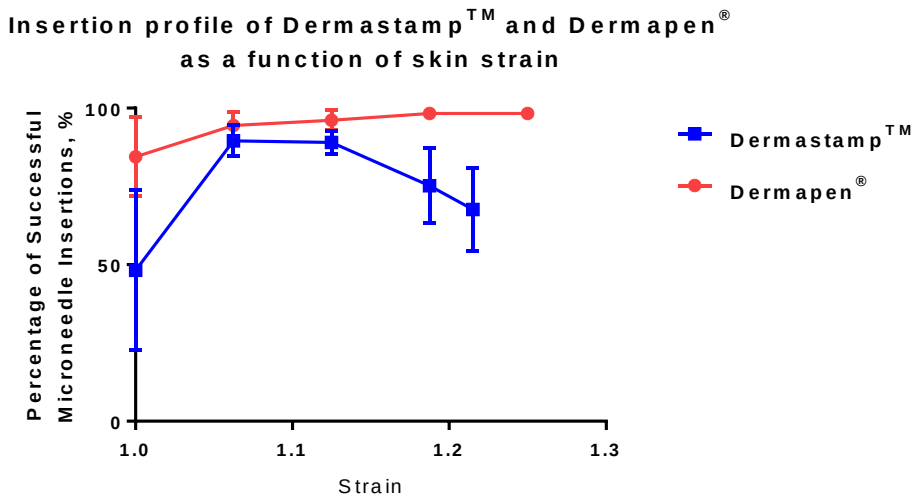

Figure 5 Averaged percentage of maximum number of dyed microneedle insertion holes generated for each level of stretch. Data expressed as means ± SD, n=5

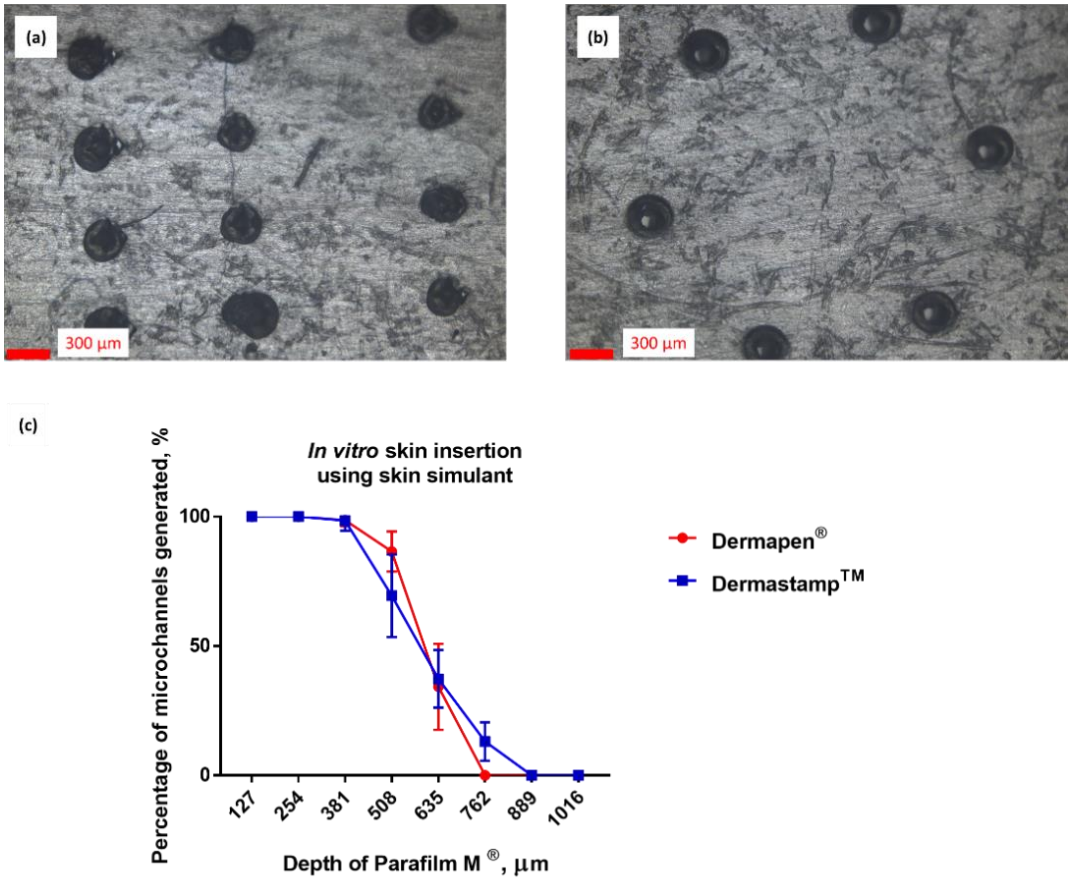

537

538 Figure 6 Microscopic images of first layer of Parafilm M® stack punctured by stainless steel
539 microneedles by (a) Dermapen®, (b) Dermastamp™ Scale bar:300 µm (c)Insertion profile of different
540 commercial microneedle systems, Dermapen® and Dermastamp™ into Parafilm M® layers, data
541 expressed as means ± SD, n=6.

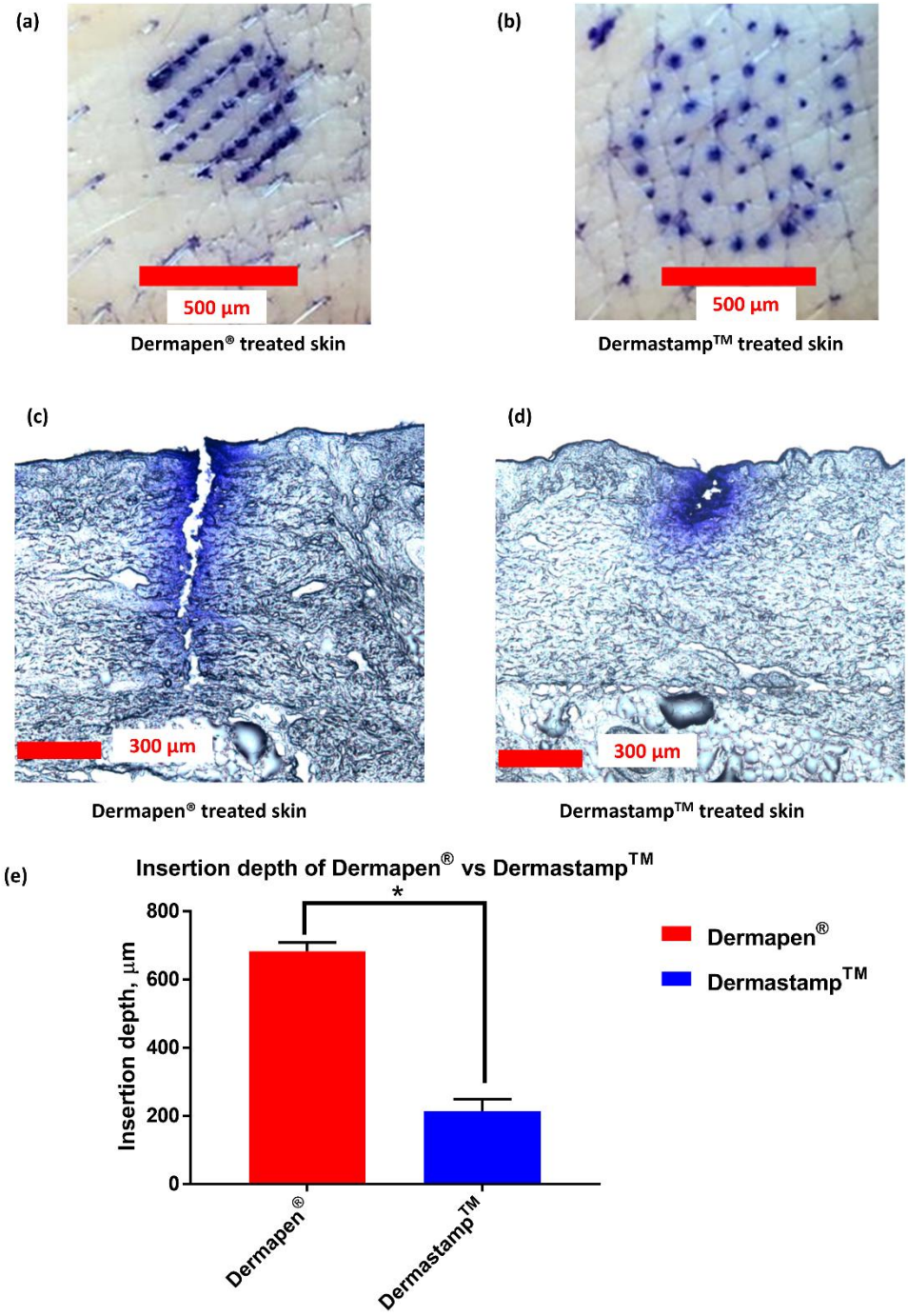

542

543 Figure 7 Visual image of porcine flank skin surface after gentian staining following (a) Dermapen® and
544 (b) Dermastamp™ application. Optical microscopy images of porcine flank skin cross sections after
545 application of (c) Dermapen and (d) Dermastamp. The skin was stained with 1% gentian violet solution
546 to allow visualisation of microneedle channels formed after microneedle treatment. n=10, data is
547 expressed as mean ± SEM.

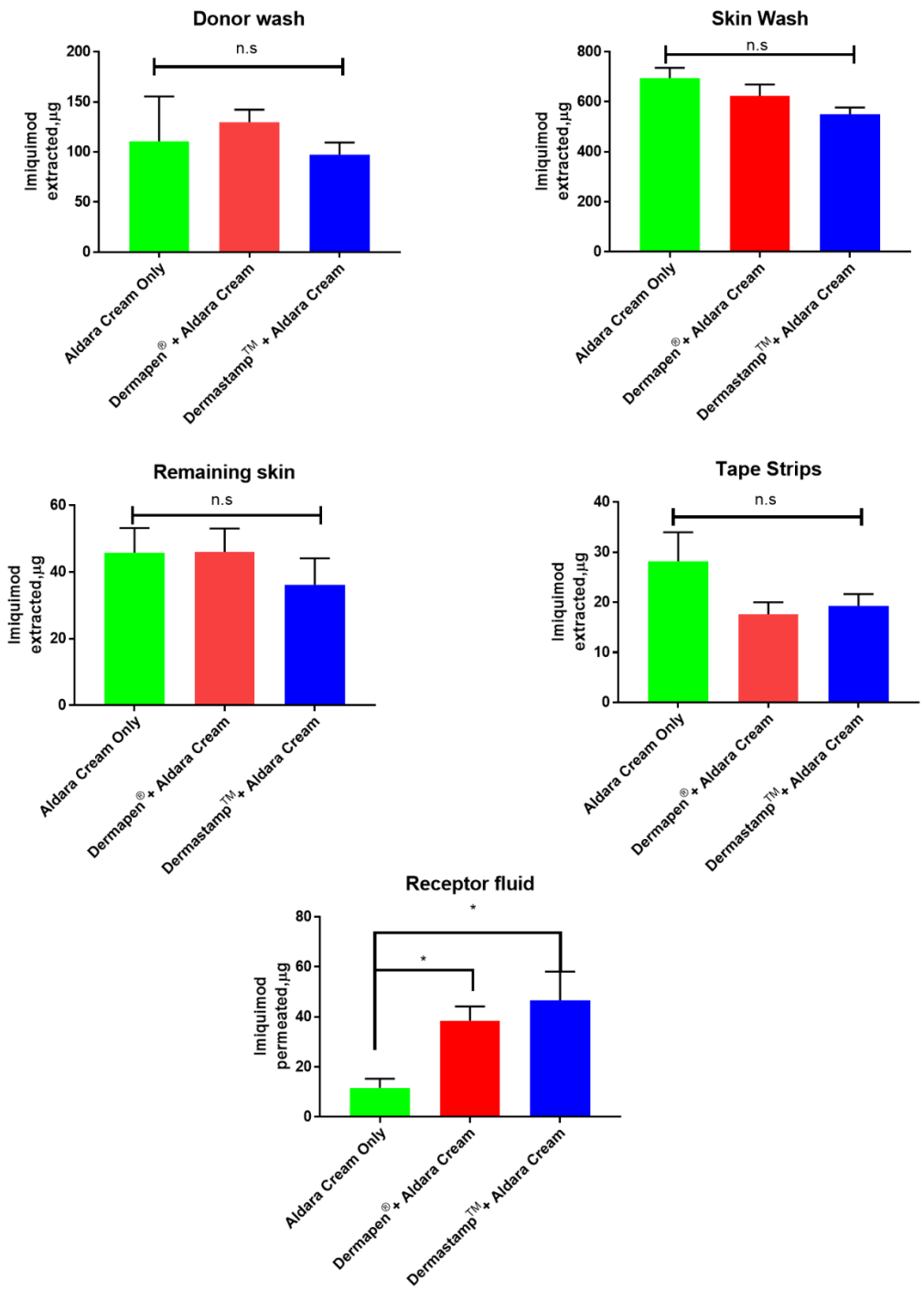

548

549 Figure 8 HPLC analysis of the mean amount of imiquimod recovered from the different Franz cell
550 components (donor chamber wash, skin wash, tape strips, remaining skin and receptor fluid) post-
551 permeation study. Data is presented as the mean ± SEM (n = 6). Differences were calculated using
552 one-way ANOVA, followed by Tukey's post hoc test, and deemed significant at $p<0.05$. n.s = not
553 statistically significant at $p>0.05$